**10976** *Inorg. Chem.* **2009**, *48*, 10976–10987
DOI: 10.1021/ic900838j

Inorganic Chemistry
Article

# Selective Chelation of Cd(II) and Pb(II) versus Ca(II) and Zn(II) by Using Octadentate Ligands Containing Pyridinecarboxylate and Pyridyl Pendants

**Raquel Ferreirós-Martínez, David Esteban-Gómez,* Carlos Platas-Iglesias, Andrés de Blas, and Teresa Rodríguez-Blas***

*Departamento de Química Fundamental, Universidade da Coruña, Campus da Zapateira, Alejandro de la Sota 1, 15008 A Coruña, Spain*

Received April 30, 2009

Herein we report the coordination properties toward Cd(II), Pb(II), Ca(II), and Zn(II) of a new octadentate ligand (py-$H_2$bcpe) based on a ethane-1,2-diamine unit containing two picolinate and two pyridyl pendants, which is structurally derived from the previous reported ligand bcpe. Potentiometric studies have been carried out to determine the protonation constants of the ligand and the stability constants of the complexes with these cations. The introduction of the pyridyl pendants in bcpe provokes a very important increase of the log$K_{ML}$ values obtained for the Pb(II) and Cd(II) complexes, while this effect is less important in the case of the Zn(II) analogue. As a result, py-bcpe shows a certain selectivity for Cd(II) and Pb(II) over Zn(II) while keeping good Pb(II)/Ca(II) and Cd(II)/Ca(II) selectivities, and the new receptor py-bcpe can be considered as a new structural framework for the design of novel Cd(II) and Pb(II) extracting agents. Likewise, the stabilities of the Cd(II) and Pb(II) complexes are higher than those of the corresponding EDTA analogues. The X-ray crystal structure of [Zn(py-bcpe)] shows hexadentate binding of the ligand to the metal ion, the coordination polyhedron being best described as a severely distorted octahedron. However, the X-ray crystal structure of the Pb(II) analogue shows octadentate binding of the ligand to the metal ion. A detailed investigation of the structure in aqueous solution of the complexes by using nuclear magnetic resonance (NMR) techniques and density functional theory (DFT) calculations (B3LYP) shows that while in the Zn(II) complex the metal ion is six-coordinated, in the Pb(II) and Ca(II) analogues the metal ions are eight-coordinated. For the Cd(II) complex, our results suggest that in solution the complex exists as a mixture of seven- and eight-coordinated species. DFT calculations performed both in the gas phase and in aqueous solution have been also used to investigate the role of the Pb(II) lone pair in the structure of the [Pb(py-bcpe)] complex.

## Introduction

The coordination chemistry of cadmium and lead is the subject of great interest due to the widespread industrial uses of their compounds and due to their inherent toxicity and health effects.[1,2] Food products account for most of the human exposure to cadmium except for areas in the vicinity of cadmium-emitting industries. Cadmium is taken up by roots of plants and passes to edible leaves, fruits, and seeds.[3] Therefore people are exposed to cadmium upon the consumption of cadmium containing plants or animals.[4] Exposure to Cd(II) causes bone diseases and gastrointestinal and renal dysfunction, and both the metal and its compounds are regarded as carcinogenic to humans.[5] Most lead poisoning results from exposure to divalent or inorganic lead, Pb(II), from inhalation or ingestion. The amount of lead in food has been reduced since 1990 due to the decline in production of some goods, the use of unleaded fuel, and other environmental protection measures. Even so, lead pollution is still an important problem in certain areas. Once ingested through the gastrointestinal track, lead accumulates in soft tissues including vital organs such as liver, kidneys, or brain, where is bound to thiol and phosphate groups in nucleic acids, proteins, and cell membranes[6−12] causing severe neurological and/or hematological effects.[13−16]

*To whom correspondence should be addressed. E-mail: mayter@udc.es (T.R.-B.), desteban@udc.es (D.E.-G.).

(1) Harrison, R. M.; Laxen, D. R. H. *Lead Pollution*; Chapman and Hall: London, 1981.
(2) (a) Nordberg, G. F. *BioMetals* **2004**, *17*, 485–489. (b) Daher, R. T. *Anal. Chem.* **1995**, *67*, 405–410.
(3) Satarug, S.; Baker, J. R.; Urbenjapol, S.; Haswell-Elkins, M.; Reilly, P. E. B.; Williams, D. J.; Moore, M. R. *Toxicol. Lett.* **2003**, *137*, 65–83.
(4) Reeves, P. G.; Chaney, R. L. *Sci. Total Environ.* **2008**, *398*, 13–19.
(5) Goyer, R. A.; Liu, J.; Waalkes, M. P. *Biometals* **2004**, *17*, 555–558.
(6) Sigel, H.; Da Costa, C. P.; Martin, R. B. *Coord. Chem. Rev.* **2001**, *219−221*, 435–461.
(7) Sigel, H.; Fischer, B. E.; Farkas, E. *Inorg. Chem.* **1983**, *22*, 925–934.
(8) Tajimir-Riahi, H. A.; Langlais, M.; Savoie, R. *Nucleic Acids Res.* **1988**, *16*, 751–762.
(9) (a) Kazantis, G. *Poisoning, Diagnosis and Treatment*; Vale, J. A., Meredith, T. J., Eds.; Update Books: London, 1981; pp 171−175. (b) Baltrop, D. *Poisoning, Diagnosis and Treatment*; Vale, J. A., Meredith, T. J., Eds.; Update Books: London, 1981; pp 178−185.
(10) Da Costa, C. P.; Siegel, H. *Inorg. Chem.* **2000**, *39*, 5985–5993.
(11) Martin, R. B. *Inorg. Chim. Acta* **1998**, *283*, 30–36.
(12) Magyar, J. S.; Weng, T.-C.; Stern, C. M.; Dye, D. F.; Rous, B. W.; Payne, J. C.; Bridgewater, M. A.; Mijovilovich, B.; Parkin, G.; Zaleski, J. M.; Penner-Hahn, J. E.; Godwin, H. A. *J. Am. Chem. Soc.* **2005**, *127*, 9495–9505.


Published on Web 10/30/2009

An important field of application of chelate-forming compounds is the removal of toxic heavy metal contaminants from aqueous waste streams by using solvent extraction or treatment with cation exchange resins. Solvent extraction occurs when a metal ion associates with an organic complexant to form a species that is transferred from the aqueous to the organic phase in a two phase system,[17] whereas cation exchange resins are formed by a polymeric skeleton functionalized with a complexant agent capable of binding to the desired metal ion;[18] therefore, these two methods require the presence of a selective complexant agent.[17,18]

A second field of application of chelate-forming compounds with toxic metal ions is the removal of these ions from living organisms.[19] Indeed, extensive clinical experience demonstrated that the prognosis in acute and chronic intoxications with a range of metal ions can be improved considerably by administration of a suitable chelating agent.[20] Ethylenediaminetetraacetic acid (EDTA), 2,3-mercaptopropanol (BAL), dimercaptosuccinic acid (DMSA), and diethylenetriaminepentaacetic acid (DTPA) are the chelating agents widely used for removal of metal toxicity.[20] An important requirement for a ligand to be used in chelation treatment of metal intoxication is a high selectivity for the metal ion to be removed with respect to those essential in the vital processes (e.g., Zn(II), Cu(II), and Ca(II)).[21] However, most of the chelating agents available for chelation treatment suffer from some side effects, such as poor selectivity and high toxicity.[21]

Aiming to get new structural frameworks with high selectivity for Pb(II) and Cd(II) over Zn(II) and Ca(II), we recently designed the ligands bcpe and bcpc, shown in Chart 1, and studied their coordinating properties toward these four metal ions.[22] We found that, although both bcpe and bcpc show important Pb/Ca and Cd/Ca selectivities, however, they are not selective for Pb(II) and/or Cd(II) over Zn(II). As a continuation of these studies and trying to increase selectivity versus Zn(II) while maintaining a good Pb/Ca and Cd/Ca selectivity, herein we report the octadentate ligand py-$H_2$bcpe (Scheme 1), structurally derived from the hexadentate bcpe by introduction of two pyridylmethyl pendants in its backbone. The py-$H_2$bcpe ligand presents several features that are expected to provide selectivity for Pb(II) and Cd(II) over Zn(II): (i) The ligand is octadentate,

**Scheme 1.** Synthesis of Ligand py-$H_2$bcpe and Its Numbering Scheme for NMR Spectral Assignment[a]

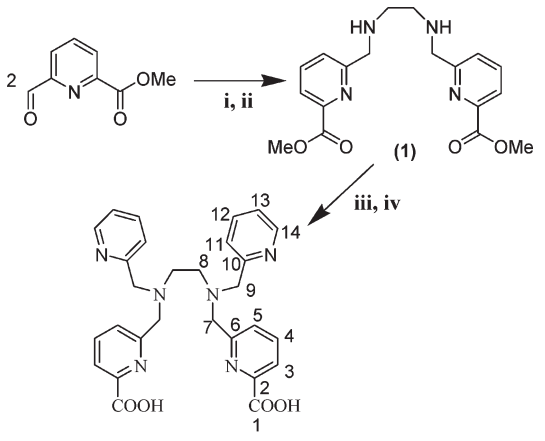


[a] (i) en, MeOH, reflux; (ii) MeOH, $NaBH_4$; (iii) 2-bromomethylpyridine, $Na_2CO_3$, $CH_3CN$; (iv) 6 M HCl, reflux.

which should favors the complexation of large metal ions such as Pb(II) and Cd(II); (ii) It is expected to form five-membered chelate rings upon metal ion coordination; the formation of five-membered chelate rings increases the selectivity for larger relative to smaller metal ions;[23] (iii) It contains pyridine units, which are known to provide strong binding to both Cd(II) and Pb(II).[24] Thermodynamic stability constants of the Ca(II), Zn(II), Cd(II), and Pb(II) complexes of py-$H_2$bcpe have been determined by pH-potentiometric titrations, while a structural analysis of the corresponding complexes has been carried out in $D_2O$ solution and solid state, also supported by a theoretical study of the [M(py-$H_2$bcpe)] systems (M = Ca, Zn, Cd, or Pb) by means of density functional theory (DFT) calculations (B3LYP model). Likewise, these DFT calculations have been also used to better understand the structural features and electronic properties related to the stereochemical activity of the Pb(II) lone pair, which is well-known to have a determinant role in the geometries of these metal complexes.

## Results and Discussion

**Synthesis of the Ligand.** Ligand py-$H_2$bcpe was obtained in four steps from methyl-6-formylpyridine-2-carboxylate (see Scheme 1), which in turn can be obtained from commercially available pyridine-2,6-dicarboxylic acid in three steps involving partial reduction of dimethyl pyridine-2,6-dicarboxylate followed by oxidation with $SeO_2$ (67% overall isolated yield).[25,26] Methyl-6-formylpyridine-2-carboxylate was reacted with ethane-1,2-diamine to give a Shiff-base intermediate, which was reduced

(13) Christensen, J. M.; Kristiansen, J. *Handbook of Metals in Clinical and Analytical Chemistry*; Seiler, H. G., Sigel, A., Sigel, H., Eds.; Marcel Dekker: New York, 1994; pp 425−440.
(14) Goyer, R. A. *Handbook on Toxicity of Inorganic Compounds*; Seiler, H. G., Sigel, A., Sigel, H., Eds.; Marcel Dekker: New York, 1988; pp 359−382.
(15) Lanphear, B. P.; Hornung, R.; Khoury, J.; Yolton, K.; Baghurst, P.; Bellinger, D. C.; Canfield, R. L.; Dietrich, K. N.; Bornschein, R.; Greene, T.; Rothenberg, S. J.; Needleman, H. L.; Schnaas, L.; Wasserman, G.; Graziano, J.; Roberts, R. *Environ. Health Perspect.* **2005**, *113*, 894–899.
(16) Castellino, C.; Caselino, P.; Sannolo, N. *Inorganic Lead Exposure: Metabolism and Intoxication*; Lewis: Boca Raton, FL, 1994.
(17) (a) Yordanov, A. T.; Roundhill, D. M. *Coord. Chem. Rev.* **1998**, *170*, 93–124. (b) Tasker, P. A.; Tong, C. C.; Westra, A. N. *Coord. Chem. Rev.* **2007**, *251*, 1868–1877.
(18) Cuenot, F.; Meyer, M.; Bucaille, A.; Guilard, R. *J. Mol. Liq.* **2005**, *118*, 89–99.
(19) Blanusa, M.; Varnai, V. M.; Piasek, M.; Kostial, K. *Curr. Med. Chem.* **2005**, *12*, 2771–2794.
(20) Andersen, O. *Chem. Rev.* **1999**, *99*, 2683–2710.
(21) Aposhian, H. V.; Maiorino, R. M.; Gonzalez-Ramirez, D.; Zuniga-Charles, M.; Xu, Z.; Hurlbut, K. M.; Junco-Munoz, P.; Dart, R. C.; Aposhian, M. M. *Toxicology* **1995**, *97*, 23–38.
(22) Ferreiros-Martinez, R.; Esteban-Gomez, D.; Platas-Iglesias, C.; de Blas, A.; Rodriguez-Blas, T. *Dalton Trans.* **2008**, 5754–5765.
(23) Gan, W.; Jones, S. B.; Reibenspies, J. H.; Hancock, R. D. *Inorg. Chim. Acta* **2005**, *358*, 3958–3966.
(24) (a) Blake, A. J.; Bencini, A.; Caltagirone, C.; De Filippo, G.; Dolci, L. S.; Garau, A.; Isaia, F.; Lippolis, V.; Mariani, P.; Prodi, L.; Montalti, M.; Zaccheroni, N.; Wilson, C. *Dalton Trans.* **2004**, 2771–2779. (b) Bazzicalupi, C.; Bencini, A.; Faggi, E.; Garau, A.; Giorgi, C.; Lippolis, V.; Perra, A.; Valtancoli, B. *Dalton Trans.* **2006**, 1409–1418. (c) Freiria, A.; Bastida, R.; Valencia, L.; Macias, A.; Lodeiro, C.; Adams, H. *Inorg. Chim. Acta* **2006**, *359*, 2383–2394.
(25) Platas-Iglesias, C.; Mato-Iglesias, M.; Djanashvili, K.; Muller, R. N.; Vander Elst, L.; Peters, J. A.; de Blas, A.; Rodríguez-Blas, T. *Chem.—Eur. J.* **2004**, *10*, 3579–3590.
(26) Chrystal, E. J. T.; Couper, L.; Robins, D. J. *Tetrahedron* **1995**, *51*, 10241–10252.

**Table 1.** Ligand Protonation Constants and Thermodynamic Stability Constants of py-bcpe and Its Metal Complexes As Determined by pH-Potentiometry[a]

| | py-bcpe[b] | bcpe[c] | bcpc[c] | edta[d] | bped[e] | dpaea[f] | edamp[g] | tpen[h] |
|---|---|---|---|---|---|---|---|---|
| log $K_1$ | 10.15(1) | 8.69 | 9.13 | 10.19 | 8.84 | 8.15 | 8.23 | 7.38 |
| log $K_2$ | 7.32(2) | 6.18 | 6.44 | 6.13 | 5.63 | 3.5 | 5.45 | 4.84 |
| log $K_3$ | 5.23(4) | 3.08 | 3.25 | 2.69 | 3.02 | 2.6 | 1.81 | 3.24 |
| log $K_4$ | 3.59(5) | 2.33 | 2.40 | 2.00 | 2.34 | | 1.62 | 2.82 |
| log $K_5$ | 1.99(6) | | | | | | | |
| log $K_{ZnL}$ | 18.14(1) | 15.62 | 15.87 | 16.5 | 15.2 | | 11.5 | 18.0 |
| log $K_{ZnHL}$ | 4.018(2) | | | | | | | |
| log $K_{CdL}$ | 20.070(1) | 14.45 | 15.89 | 16.5 | 14.6 | | 9.9 | 16.6 |
| log $K_{CdHL}$ | 3.47(2) | | | | | | | |
| log $K_{PbL}$ | 18.87(2) | 12.68 | 15.00 | 18.0 | | 12.1 | | 14.3 |
| log $K_{PbHL}$ | 4.07(4) | | | | | | | |
| log $K_{CaL}$ | 14.48(1) | 5.81 | 6.07 | 10.6 | | 5.5 | | 4.4 |
| log $K_{CaHL}$ | 4.34(2) | | | | | | | |
| log $K_{CaH2L}$ | 4.14(1) | | | | | | | |

[a] $I$ = 0.1 M ($Me_4N$)($NO_3$). Data reported previously for related systems are provided for comparison. [b] This work. [c] Reference 22. [d] References 27 and 28. [e] Reference 29. [f] Reference 30. [g] Reference 31. [h] Reference 28.

**Chart 1**

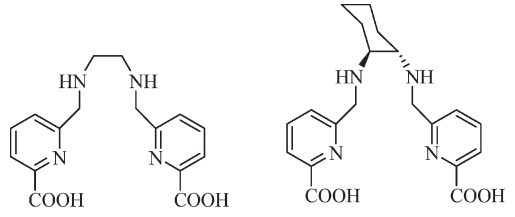


$H_2$bcpe $H_2$bcpc

with sodium tetrahydroborate to give amine **1**.[25] Compound **1** was then reacted with 2-bromomethylpyridine in $CH_3CN$ solution in the presence of $Na_2CO_3$. The ligand was finally obtained by hydrolysis of the methylester groups in 6 M HCl as py-$H_2$bpce·4HCl·3$H_2O$ in ~14% overall yield calculated from commercially available pyridine-2,6-dicarboxylic acid. The low solubility of $PbCl_2$ prevents the use of the ligand as its hydrochloride salt for Pb(II) complexation studies. Thus, py-$H_2$bpce·4HCl·3$H_2O$ was reacted with a stoichiometric amount of $Ag(NO_3)$ to give py-$H_2$bpce·4$HNO_3$·4$H_2O$.

**Ligand Protonation Constants and Stability Constants of the Metal Complexes.** The protonation constants of py-bcpe as well as the stability constants of its metal complexes formed with the cations Zn(II), Cd(II), Pb(II), and Ca(II) were determined by potentiometric titrations. The constants and standard deviations are given in Table 1, which also lists the protonation and stability constants reported for the related systems bcpe and bcpc (Chart 1),[22] and edta,[27,28] bped,[27,29] dpaea,[30] edamp,[31] and tpen[28] (Chart 2). The ligand protonation constants

**Chart 2**

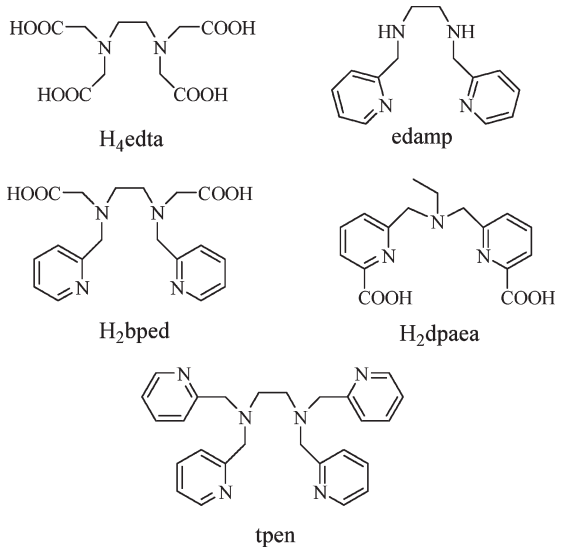


$H_4$edta edamp $H_2$bped $H_2$dpaea tpen

are defined as in eq 1, and the stability constants and protonation constants of the metal complexes are expressed in eqs 2 and 3 (L = py-bcpe):

$$K_i = \frac{[H_iL]}{[H_{i-1}L][H^+]} \quad (1)$$

$$K_{ML} = \frac{[ML]}{[M][L]} \quad (2)$$

$$K_{MH_iL} = \frac{[MH_iL]}{[MH_{i-1}L][H^+]} \quad (3)$$

In comparison to bcpe, py-bcpe has higher protonation constants for the first and second protonation steps, which occur on the amine nitrogen atoms. Thus, the introduction of the 2-pyridylmethyl pendant arms appears to cause an increase of the basicity of the amine nitrogen atoms. This effect also accounts for the increased basicity of py-bcpe in comparison to edamp. However, the opposite effect is observed when comparing the log $K_1$ and log $K_2$ values reported for edamp and tpen. The UV−vis absorption spectra of py-bcpe recorded at different pH values confirm that a protonation process occurs above pH 8.5 (Figure S2, Supporting Information). These results are in contrast to previous findings, which indicated that the introduction of pyridyl pendants results in a reduced basicity of the amine nitrogen atoms.[32] Although we do not have a definitive explanation for the increased basicity of the amine nitrogen atoms upon introduction of 2-pyridylmethyl groups to bcpe, this could be related to a different ability of the pyridyl versus picolinate groups to form internal hydrogen bonds with the protonated nitrogens. A comparison of the protonation constants determined for py-bcpe,

(27) Lacoste, R. G.; Christoffers, G. V.; Martell, A. E. *J. Am. Chem. Soc.* **1965**, *87*, 2385–2388.
(28) Martell, A. E.; Motekaitis, R. J.; Smith, R. M. *NIST Critically Selected Stability Constants of Metal Complexes Database*, version 8.0 for Windows; Standard Reference Data Program, National Institute of Standards and Technology: Gaithersburg, MD, **2004**.
(29) Caravan, P.; Rettig, S. J.; Orvig, C. *Inorg. Chem.* **1997**, *36*, 1306–1315.
(30) Pellissier, A.; Bretonniere, Y.; Chatterton, N.; Pecaut, J.; Delangle, P.; Mazzanti, M. *Inorg. Chem.* **2007**, *46*, 3714–3725.
(31) Lacoste, R. G.; Martell, A. E. *Inorg. Chem.* **1964**, *3*, 881–884.
(32) Miyake, H.; Watanabe, M.; Takemura, M.; Hasegawa, T.; Kojima, Y.; Inoue, M. B.; Inoue, M.; Fernando, Q. *J. Chem. Soc., Dalton Trans.* **2002**, 1119–1125.

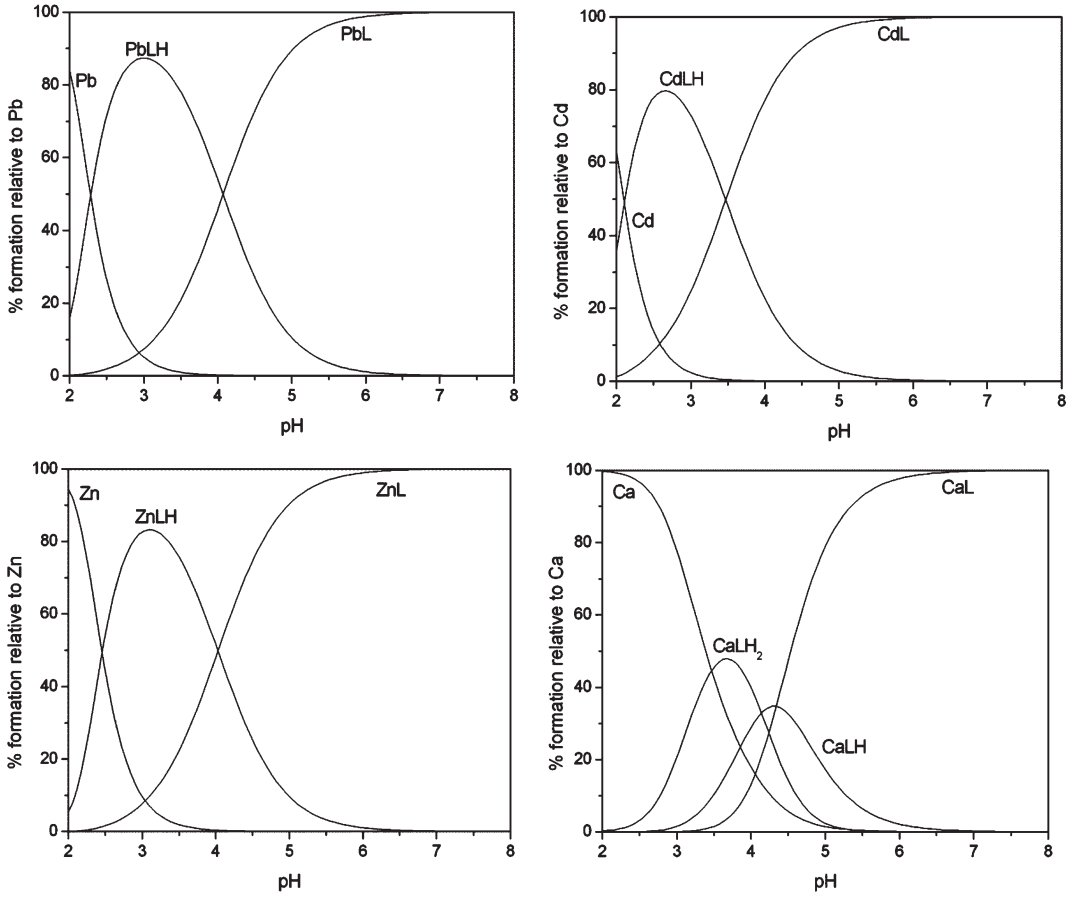


**Figure 1.** Lead, cadmium, zinc, and calcium speciation in the presence of py-bcpe; $[M^{2+}]_{tot} = [L]_{tot} = 10^{-3}$ M; $I = 0.1$ M $(Me_4N)(NO_3)$.

bcpe, dpaea, and edamp shows that the third and fourth protonation steps in py-bcpe probably take place at the carboxylate groups.[33,34] However, the introduction of the pyridyl pendants appears to provoke a considerable increase of the basicity of the picolinate groups. Finally, the last protonation process probably occurs on a nitrogen atom of a pyridyl pendant.

The 1:1 titration curves of $H_2$py-bcpe·4HCl with Ca(II), Zn(II), or Cd(II) and $H_2$py-bcpe·4$HNO_3$ with Pb(II) (Figure S1, Supporting Information) display an inflection at $a = 6$ ($a$ = moles of $OH^-$/moles of ligand), as expected for the formation of [M(py-bcpe)] species (M = Pb, Cd, Zn, or Ca). The potentiometric data do not indicate the presence of significant amounts of soluble hydroxide complexes in the pH range investigated. Monoprotonated forms of the py-bcpe complexes have been detected over the pH range studied for the Zn(II), Cd(II), and Pb(II) complexes, while for the Ca(II) analogue both mono- and diprotonated forms of the complex were observed. The species distribution diagrams obtained for the different complexes of py-bcpe are shown in Figure 1. The diagrams obtained for Zn(II) and Pb(II) show the presence of a monoprotonated complex in solution at pH < 6, while the dissociation of the complex occurs below pH ~4.0. In the case of the Cd(II) complex, the protonation of the complex starts at lower pH (~5.5), while the dissociation of the complex is observed at pH < 3.5. For the Ca(II) complex, dissociation starts already at pH < 5, which indicates that this complex is considerably less stable than the Zn(II), Cd(II), and Pb(II) analogues.

The introduction of the pyridyl pendants provokes a very important increase of the log $K_{ML}$ values obtained for the Pb(II) and Cd(II) complexes, while this effect is less important in the case of the Zn(II) analogue [log $K_{M(py\text{-}bcpe)}$ − log $K_{M(bcpe)}$ = 6.2 (Pb), 5.6 (Cd), and 2.5 (Zn)]. As a consequence, the log $K_{ML}$ values determined for py-bcpe follow the trend Cd(II) > Pb(II) > Zn(II). This is in contrast to the trend observed for bcpe and tpen complexes, for which the Zn(II) complex shows the highest stability among these three metal ions.[22] Most of the increase in stability of the Zn(II) complex upon introduction of the pyridyl pendants is due to the greater basicity of py-bcpe ($\Sigma$ log{[$H_i$py-bcpe]/[$H_{i-1}$py-bcpe][$H^+$]} = 26.3, $i$ = 1−4) over that of bcpe ($\Sigma$log{[$H_i$bcpe]/[$H_{i-1}$bcpe][$H^+$] = 20.3, $i$ = 1−4), as the solid state structure of [Zn(py-bcpe)] shows that the pyridyl pendant arms do not participate in the coordination to the metal ion. The introduction of the pyridyl pendants also results in a dramatic increase of log $K_{CaL}$, but even so the py-bcpe ligand maintains a good Cd/Ca and Pb/Ca selectivity. The stability of the Ca(II) complex of py-bcpe is also considerably higher than that of tpen, which is attributed to the presence of two negatively charged carboxylate groups in py-bcpe. The speciation diagrams shown in Figure 1 highlight the selectivity of py-bcpe for Pb and Cd over Ca. For instance nearly all the Cd(II) and Pb(II) is complexed at pH

(33) Chatterton, N.; Gateau, C.; Mazzanti, M.; Pécaut, J.; Borel, A.; Helm, L.; Merbach, A. *Dalton Trans.* **2005**, 1129–1135.
(34) Roca Sabio, A.; Mato-Iglesias, M.; Esteban-Gomez, D.; Toth, E.; de Blas, A.; Platas-Iglesias, C.; Rodríguez-Blas, T. *J. Am. Chem. Soc.* **2009**, *131*, 3331–3341.

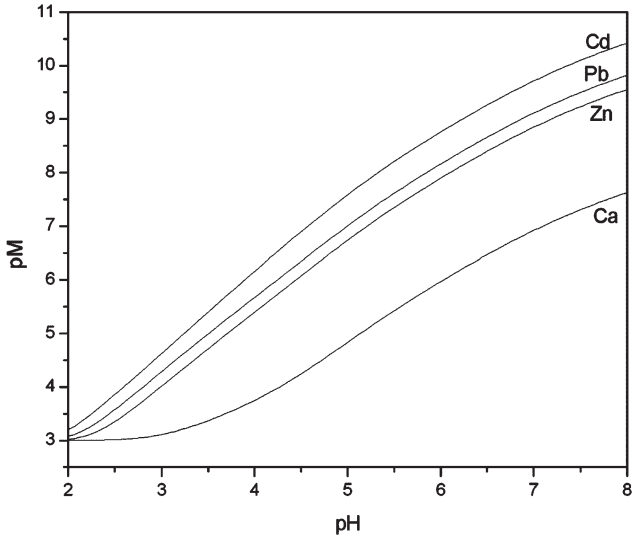


**Figure 2.** pM = $-\log[M(II)]_{free}$ as a function of pH calculated in aqueous solution for py-bcpe complexes; $[M^{2+}]_{tot} = [L]_{tot} = 10^{-3}$ M.

3.0 (97.6% and 95.2%, respectively), while only 22.4% of the total Ca(II) is complexed under the same conditions. In order to better demonstrate the selectivity of py-bcpe, we have calculated the residual free M(II) concentration in solution (Figure 2), since the comparison of stability constants of complexes with different stoichiometry is meaningless. The inspection of the pM = $-\log[M(II)]_{free}$ values confirm the stability of the py-bcpe complexes follows the trend Cd(II) > Pb(II) > Zn(II) ≫ Ca(II). Interestingly, the log $K_{ML}$ values obtained for all py-bcpe complexes investigated in this work are higher than those reported for the corresponding edta complexes (Table 1).

**Structure of the Complexes.** The $^1$H and $^{13}$C NMR spectra of the Zn(II), Cd(II), Pb(II), and Ca(II) complexes of py-bcpe were recorded from $D_2O$ solution at 298 K and assigned on the basis of two-dimensional correlation spectroscopy (COSY), heteronuclear single quantum coherence (HSQC), and heteronuclear multiple bond coherence (HMBC) experiments (see Scheme 1 for labeling). The results are summarized in Table 2.

The $^1$H NMR spectra of the Ca(II) and Pb(II) complexes are quite similar (Figure 3). They show seven signals for the aromatic protons of the ligand, while the H9ax/H9eq protons give an AB spin pattern, and the protons of the ethylenediamine units H8ax/H8eq give an AA′BB′ spectrum. The signals due to H7ax and H7eq protons are observed as a singlet for both complexes at this temperature. Although the specific $CH_2$ proton assignments of the axial and equatorial H8−H9 protons were not possible on the basis of the 2D NMR spectra, they were carried out using the stereochemically dependent proton shift effects, resulting from the polarization of the C−H bonds by the electric field effect caused by the cation charge. This results in a deshielding effect of the equatorial protons, which are pointing away from the metal ion.[35,36] The $^{13}$C NMR spectra of both complexes show 14 NMR peaks for the 28 carbon nuclei of the ligand backbone (Table 2), in agreement with an effective $C_2$ symmetry of the complexes in solution. The formation of the complex provokes important downfield shifts of protons H3, H4, and H5, which indicates the coordination of the picolinate pendants in both complexes. Protons H14 experience an important upfield shift upon

**Table 2.** $^1$H and $^{13}$C NMR Shifts for Ligand py-bcpe and Its Ca(II) and Pb(II) Complexes (See Scheme 1 for Labeling)[a]

| | py-bcpe | Pb[b] | Ca[c] |
|---|---|---|---|
| H3 | 7.69 | 7.98 | 8.05 |
| H4 | 7.67 | 8.02 | 8.05 |
| H5 | 7.32 | 7.56 | 7.46 |
| H7eq | 3.75 | 4.08 | 3.79 |
| H7ax | 3.75 | 4.08 | 3.79 |
| H8eq | 2.60 | 3.09 | 2.78 |
| H8ax | 2.60 | 2.95 | 2.42 |
| H9eq | 3.70 | 3.99 | 3.73 |
| H9ax | 3.70 | 3.89 | 3.49 |
| H11 | 7.28 | 7.37 | 7.09 |
| H12 | 7.66 | 7.68 | 7.67 |
| H13 | 7.22 | 6.97 | 7.11 |
| H14 | 8.27 | 7.68 | 7.97 |
| C1 | 174.4 | 173.2 | 174.0 |
| C2 | 154.5 | 154.1 | 153.3 |
| C3 | 124.0 | 126.3 | 124.6 |
| C4 | 139.8 | 141.6 | 142.0 |
| C5 | 127.0 | 127.9 | 126.7 |
| C6 | 158.5 | 158.0 | 159.6 |
| C7 | 61.8 | 61.1 | 60.1 |
| C8 | 52.6 | 54.1 | 55.6 |
| C9 | 61.8 | 61.9 | 62.8 |
| C10 | 158.1 | 158.4 | 157.0 |
| C11 | 126.1 | 126.1 | 126.5 |
| C12 | 139.5 | 140.8 | 139.8 |
| C13 | 124.7 | 125.5 | 124.9 |
| C14 | 149.6 | 149.8 | 150.2 |

[a] Conditions: $T$ = 298 K, $D_2O$, 300 MHz, pD = 7.0. Assignment supported by 2D H,H COSY, HSQC, and HMBC experiments. See Scheme 1 for labeling. [b] $^3J_{5-4}$ = 6.9 Hz; $^3J_{11-12}$ = 6.9 Hz; $^2J_{9ax\text{-}9eq}$ = 15.0 Hz. [c] $^2J_{8ax\text{-}8eq}$ = 10.3 Hz; $^2J_{9ax\text{-}9eq}$ = 14.5 Hz; $^3J_{5-4}$ = 5.6 Hz; $^4J_{5-3}$ = 3.1 Hz.

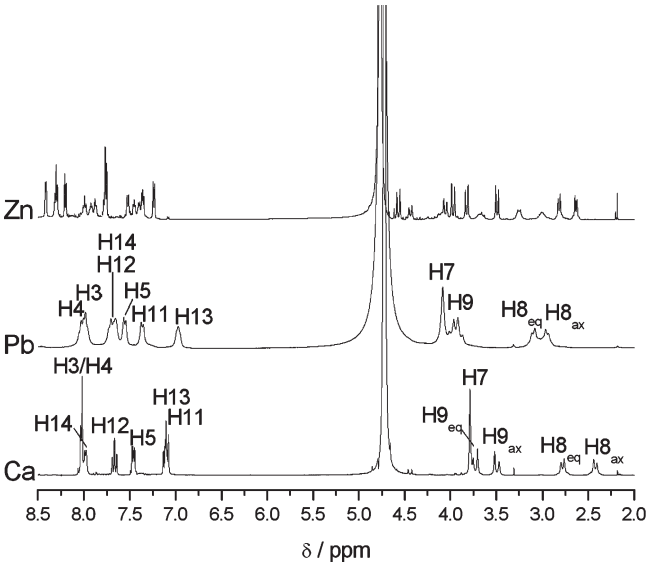


**Figure 3.** $^1$H NMR spectra of the Zn, Pb, and Ca complexes of py-bcpe as recorded in $D_2O$ solution at 298 K (pD = 7.0).

(35) Vaiana, L.; Regueiro-Figueroa, M.; Mato-Iglesias, M.; Platas-Iglesias, C.; Esteban-Gómez, D.; de Blas, A.; Rodríguez-Blas, T. *Inorg. Chem.* **2007**, *46*, 8271–8282.

(36) González-Lorenzo, M.; Platas-Iglesias, C.; Avecilla, F.; Geraldes, C. F. G. C.; Imbert, D.; Bünzli, J.-C. G.; de Blas, A.; Rodríguez-Blas, T. *Inorg. Chem.* **2003**, *42*, 6946–6954.

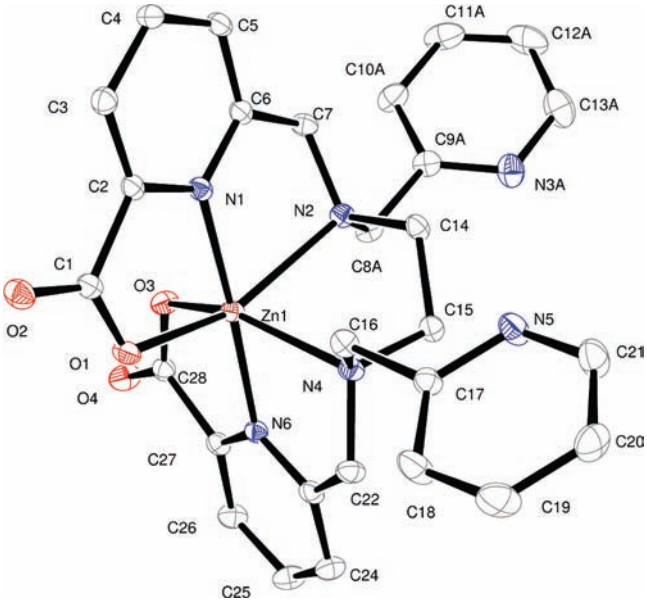


**Figure 4.** X-ray crystal structure of [Zn(py-bcpe)] with atom labeling; hydrogen atoms are omitted for simplicity. The ORTEP plot is drawn at the 50% probability level. One of the pyridyl pendants of the ligand is disordered, but only the positions with higher occupancy factors are shown for the sake of clarity.

formation of the Pb(II) and Ca(II) complexes, which suggests that the pyridyl pendants are also involved in the coordination to the metal ion.

The $^1$H NMR spectrum of the Zn(II) complex recorded at pH = 7 shows two different sets of signals with an intensity ratio of ~1.2:1.0. The two species show a spectral pattern that is consistent with an effective $C_2$ symmetry in solution. The $^1$H NMR spectrum of the major species is well resolved, while the minor species shows however broad signals for the H9ax/H9eq and H8ax/H8eq protons (Figure 3). Finally, the $^1$H NMR spectrum of the Cd(II) complex is very complex and suggests the presence of at least two different complex species in solution.

Single crystals suitable for X-ray diffraction analysis of formula [Zn(py-bcpe)]·3.83$H_2O$ (**1**) and [Pb(py-bcpe)]·2$Et_3NHClO_4$·$H_2O$ (**2**) were obtained for the Zn(II) and Pb(II) complexes, respectively. Crystals of the Zn(II) derivative contain the expected neutral complex [Zn(py-bcpe)] and noncoordinated water molecules hydrogen bonded to the oxygen atoms of the carboxylate groups. Figure 4 shows a view of the structure of the complex, while bond lengths and angles of the metal coordination environment are listed in Table 3. The metal ion is directly bound to six of the eight donor atoms of the ligand, with the coordination polyhedron around the metal ion being best described as a severely distorted octahedron. The two nitrogen atoms of the pyridyl pendants [N(5) and N(3)] remain uncoordinated. As a result, the metal coordination environment in [Zn(py-bcpe)] is very similar to that previously observed for the complex of bcpe.[22] A distorted octahedral coordination has been also observed for the $[Zn(tpen)]^{2+}$ complex.[37] A ligand such as bcpe can coordinate in an octahedral fashion to a metal ion with

**Table 3.** Bond Lengths (Å) and Angles (deg) for the Zn(II) and Pb(II) Complexes of py-bcpe[a]

| Zn | | Pb | |
|---|---|---|---|
| Zn(1)−N(1) | 2.031(2) | Pb(1)−N(1) | 2.537(2) |
| Zn(1)−N(2) | 2.323(2) | Pb(1)−N(2) | 2.594(2) |
| Zn(1)−N(4) | 2.263(2) | Pb(1)−N(3) | 2.589(2) |
| Zn(1)−N(6) | 2.041(2) | Pb(1)−N(4) | 2.856(2) |
| Zn(1)−O(1) | 2.133(1) | Pb(1)−N(5) | 2.901(2) |
| Zn(1)−O(3) | 2.121(1) | Pb(1)−N(6) | 2.790(2) |
| | | Pb(1)−O(1) | 2.693(2) |
| | | Pb(1)−O(3) | 2.709(2) |
| N(1)−Zn(1)−O(1) | 77.66(6) | N(1)−Pb(1)−O(3) | 65.71(6) |
| N(6)−Zn(1)−O(3) | 77.34(6) | N(1)−Pb(1)−N(3) | 82.95(7) |
| N(1)−Zn(1)−O(3) | 102.62(6) | N(1)−Pb(1)−N(2) | 63.51(7) |
| N(1)−Zn(1)−N(6) | 176.62(6) | N(3)−Pb(1)−N(2) | 66.82(7) |
| O(3)−Zn(1)−N(4) | 150.67(6) | N(1)−Pb(1)−O(1) | 61.89(6) |
| O(1)−Zn(1)−N(4) | 93.66(6) | N(3)−Pb(1)−O(1) | 77.89(6) |
| N(1)−Zn(1)−N(2) | 76.14(6) | N(2)−Pb(1)−O(1) | 117.15(6) |
| N(6)−Zn(1)−N(2) | 107.23(6) | O(3)−Pb(1)−N(6) | 59.43(6) |
| N(6)−Zn(1)−O(1) | 99.05(6) | N(3)−Pb(1)−O(3) | 147.72(6) |
| O(3)−Zn(1)−O(1) | 103.96(6) | N(2)−Pb(1)−O(3) | 91.22(6) |
| N(1)−Zn(1)−N(4) | 103.96(6) | O(1)−Pb(1)−O(3) | 93.04(6) |
| N(6)−Zn(1)−N(4) | 76.85(6) | N(1)−Pb(1)−N(6) | 111.10(6) |
| O(3)−Zn(1)−N(2) | 92.54(6) | N(3)−Pb(1)−N(6) | 132.20(6) |
| O(1)−Zn(1)−N(2) | 151.51(6) | N(2)−Pb(1)−N(6) | 78.98(6) |
| N(4)−Zn(1)−N(2) | 82.04(6) | O(1)−Pb(1)−N(6) | 149.57(6) |

[a] See Figures 4 and 5 for numbering scheme.

three possible geometries: *trans*(*O*,*O*), *trans*($N_{py}$,$N_{py}$), and *cis*(*O*,*O*) [this one also named as *cis*($N_{py}$,$N_{py}$)],[29] where $N_{py}$ denotes a nitrogen atom of a pyridine unit. The X-ray structure of [Zn(py-bcpe)] (Figure 4) shows that the complex adopts a *trans*($N_{py}$,$N_{py}$) conformation in the solid state, the N(1)−M(1)−N(6) angle amounting to 176.62(6)°. The two tridentate aminopicolinate moieties bind meridionally through their N-amine, N-pyridine, and O-carbonyl atoms. The meridional arrangement of the aminopicolinate moieties can be proven by the dihedral angles that the terminal donor atoms of each aminopicolinate moiety [O(1)−N(2) and O(3)−N(4)] form with the N(1)−N(6) axis. This angle, indicated as $\tau$, has ideal values of 54.7, 90, and 180° for the undistorted *u-fac*, *s-fac*, and *mer* isomers.[38] The large amount of distortion of the octahedral coordination leads to a considerable deviation from the ideal value of 180° ($\tau$ = 168.4° for O1N1−N6N2 and $\tau$ = 163.6° for O3N6−N1N4. The py-bcpe ligand forms five five-membered chelate rings imposing large distortions on the ideally octahedral coordination angles. Indeed, while the trans N(1)−Zn(1)−N(6) angle is relatively close to 180°, the *trans* angles O(1)−Zn(1)−N(2) and O(3)−Zn(1)−N(4) (~150°) markedly deviate from linearity (Table 3). The vectors defined by the metal ion and the axial donors N(1) and N(6) form angles with the vectors containing the metal ion and the equatorial donor atoms ranging from 76.14 to 107.23°, which indicates an important distortion from regular octahedral geometry of these angles (ideal value 90°).

Crystals of the Pb(II) complex were obtained from reaction of the ligand with Pb(II) perchlorate in the presence triethylamine, and they contain the expected neutral complex, water molecules hydrogen bonded to

(37) (a) Blindauer, C. A.; Razi, M. T.; Parsons, S.; Sadler, P. J. *Polyhedron* **2006**, *25*, 513–520. (b) Mikata, Y.; Wakamatsu, M.; Yano, S. *Dalton Trans.* **2005**, 545–550.

(38) (a) Rodriguez, V.; Gutierrez-Zorrilla, J. M.; Vitoria, P.; Luque, A.; Roma, P.; Martinez-Ripoll, M. *Inorg. Chim. Acta* **1999**, *290*, 57–63. (b) Meier, R.; Molinier, M.; Anson, C.; Powell, A. K.; Kallies, B.; van Eldik, R. *Dalton Trans.* **2006**, 5506–5514.

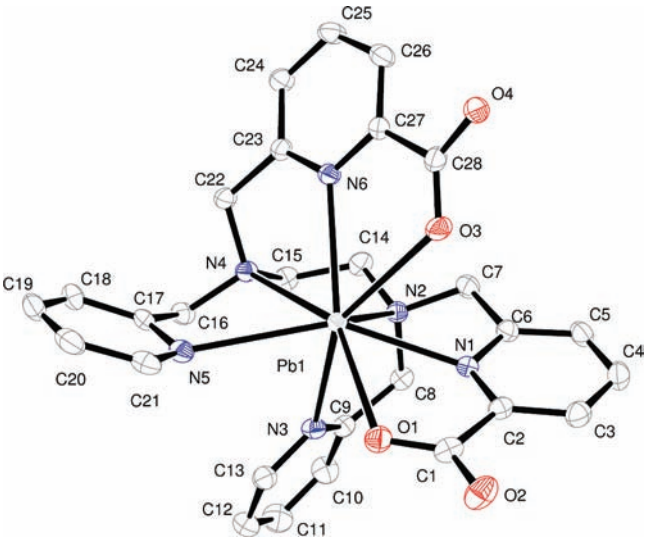


**Figure 5.** X-ray crystal structure of [Pb(py-bcpe)] with atom labeling; hydrogen atoms are omitted for simplicity. The ORTEP plot is drawn at the 50% probability level.

the oxygen atoms of the carboxylate groups, and triethylammonium perchlorate. In contrast to the situation observed for the Zn(II) analogue, in [Pb(py-bcpe)] the metal ion is directly bound to the eight donor atoms of the ligand. Therefore, the introduction of the pyridyl pendants increases the coordination number of the Pb(II) metal ion with respect to the observed in the related bcpe, where tetrameric $[Pb_4(bcpe)_4]$ units were found in the solid state with the metal ion seven-coordinated.[22] Figure 5 shows a view of the structure of the [Pb(py-bcpe)] complex, while bond lengths and angles of the metal coordination environment are listed in Table 3. The bond distances shown in Table 3 indicate an asymmetrical coordination of the metal ion by the ligand, with the Pb−N(4), Pb−N(5), and Pb−N(6) distances ($2.85 \pm 0.05$ Å) being substantially longer than the Pb−N(1), Pb−N(2), and Pb−N(3) ones ($2.57 \pm 0.04$ Å). On the other hand, it is well-known that ligands containing two methylpicolinate moieties bridged by an ethylenediamine group may adopt two different conformations depending on the relative arrangement of the two pyridine units: twist-wrap (tw), in which the ligand wraps around the metal ion by twisting the pyridyl units relative to each other, and twist-fold (tf), where the twisting of the pyridyl units is accompanied by an overall folding of the two pyridine units.[39] Inspection of the X-ray crystal structures of the Zn(II) and Pb(II) complexes shown in Figures 4 and 5 indicate that while the Zn(II) complex presents a tw conformation, the Pb(II) analogue adopts a tf arrangement in the solid state. As it can be seen in Figure 5, the disposition of the donor atoms of the ligand around the Pb(II) ion results in an identifiable void. This is typical of the so-called hemidirected compounds, in which the lone pair of electrons causes a nonspherical charge distribution around the Pb(II) cation.[40,41]

The complexes of py-bcpe present two sources of helicity: one associated with the layout of the coordinated picolinate and/or pyridyl pendant arms (absolute configuration $\Delta$ or $\Lambda$) and the other to the five-membered chelate ring formed by the binding of the ethylenediamine moiety (absolute configuration $\delta$ or $\lambda$).[42,43] Furthermore, each of the two amine nitrogen atoms becomes chiral upon coordination to the metal ion (absolute configuration *R* or *S*). Thus, a ligand such as py-bcpe can form the six possible enantiomeric pairs of diasteroisomers shown in Chart 3. Inspection of the crystal data shows that the crystal of the Zn(II) complex contains a racemic mixture of two centrosymmetrically related enantiomers [$\Lambda(\lambda)$ and $\Delta(\delta)$]. Likewise, the amine nitrogen atoms present different configurations in the Zn(II) and Pb(II) complexes. Indeed, while in the Zn(II) complex the amine nitrogen atoms adopt *RR* or *SS* configurations, as both enantiomers are present in the crystal, in the Pb(II) complex *RS* and *SR* configurations are observed. As a result, in [Pb(py-bcpe)] the two pyridyl pendant arms are placed below the plane defined by the amine nitrogen atoms [N(2) and N(4)] and the metal ion, while in the Zn(II) analogue the two pyridyl pendants are alternatively placed above and below that plane. The conformation adopted by the ligand in the Pb(II) complex is different to that observed for lanthanide complexes with related octadentate ligands, for which *RR* or *SS* configurations have been observed.[25,39,44]

With the aim to obtain more information about the structure in solution of the [M(py-bcpe)] complexes (M = Zn, Cd, Pb, or Ca), these systems were characterized by using DFT calculations (B3LYP model). On the grounds of our previous experience,[22,41,45] in these calculations the 6-31G(d) basis set was used for the ligand atoms, while for the metals the effective core potential (ECP) of Wadt and Hay (Los Alamos ECP) included in the LanL2DZ basis set was applied.[46] Compared to all-electron basis sets, ECPs account for relativistic effects to some extent. It is believed that relativistic effects will become important for the elements from the fourth row of the periodic table. As stated above, the ligand py-bcpe can form the six possible enantiomeric pairs of diasteroisomers shown in Chart 3. The situation is further complicated by the fact that py-bcpe can form complexes with different coordination numbers depending on the particular metal ion involved in complexation. Indeed, the solid state structures of the Zn(II) and Pb(II) complexes described above show coordination numbers of six and eight, respectively. Since enantiomers have the same physicochemical properties in a nonchiral environment, we have considered up to six diasteroisomeric forms of the complexes in our

(39) Mato-Iglesias, M.; Balogh, E.; Platas-Iglesias, C.; Toth, E.; de Blas, A.; Rodríguez-Blas, T. *Dalton Trans.* **2006**, 5404–5415.
(40) Shimoni-Livny, L.; Glusker, J. P.; Bock, C. W. *Inorg. Chem.* **1998**, *37*, 1853–1867.
(41) Esteban-Gómez, D.; Platas-Iglesias, C.; Enríquez-Pérez, T.; Avecilla, F.; de Blas, A.; Rodríguez-Blas, T. *Inorg. Chem.* **2006**, *45*, 5407–5416.
(42) Jensen, K. A. *Inorg. Chem.* **1970**, *9*, 1–5.
(43) Maigut, J.; Meier, R.; Zahl, A.; van Eldik, R. *Inorg. Chem.* **2008**, *47*, 5702–5719.
(44) Mato-Iglesias, M.; Platas-Iglesias, C.; Djanashvili, K.; Peters, J. A.; Tóth, É.; Balogh, E.; Muller, R. N.; Vander Elst, L.; de Blas, A.; Rodríguez-Blas, T. *Chem. Commun.* **2005**, 4729–4731.
(45) (a) Platas-Iglesias, C.; Esteban-Gómez, D.; Enríquez-Pérez, T.; Avecilla, F.; de Blas, A.; Rodríguez-Blas, T. *Inorg. Chem.* **2005**, *44*, 2224–2233. (b) Esteban-Gómez, D.; Platas-Iglesias, C.; Avecilla, F.; de Blas, A.; Rodríguez-Blas, T. *Eur. J. Inorg. Chem.* **2007**, 1635–1643. (c) Regueiro-Figueroa, M.; Esteban-Gómez, D.; Platas-Iglesias, C.; de Blas, A.; Rodríguez-Blas, T. *Eur. J. Inorg. Chem.* **2007**, 2198–2207.
(46) Hay, P. J.; Wadt, W. R. *J. Chem. Phys.* **1985**, *82*, 270–283.

**Chart 3.** Six Possible Enantiomeric Pairs of Diasteroisomers for Octacoordinated py-bcpe Complexes

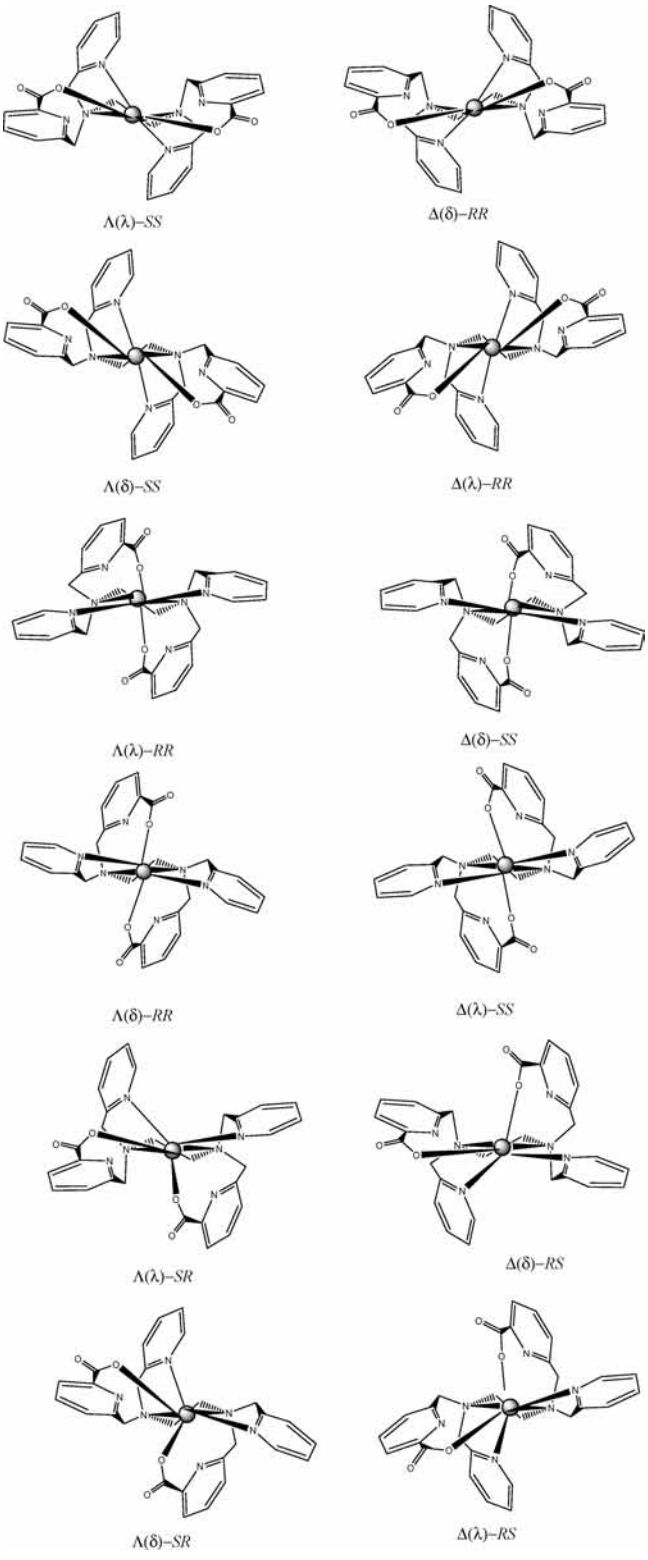


conformational analysis [Λ(λ)-*RR*, Λ(δ)-*RR*, Λ(λ)-*SS*, Λ(δ)-*SS*, Λ(λ)-*SR*, and Λ(δ)-*SR*, see Chart 3] for each plausible coordination number (6, 7, or 8). In the following, the coordination number will be indicated with the corresponding arabic number placed within parentheses (i.e., Λ(λ)-*RR*(6) indicates coordination number 6). Optimized Cartesian coordinates for the different conformations of [M(py-bcpe)] complexes are given in the Supporting Information. Full geometry optimization of each conformation performed in vacuo was followed by single point energy calculations in aqueous solution. The relative energies of the different conformations in aqueous solution are given in Table 4. According to our calculations, the Λ(λ)-*RR*(6) form is the most stable one in the case of the [Zn(py-bcpe)] complex, in nice agreement with the solid state structure of the complex described above. However, a second diasteroisomer [Λ(δ)-*RR*(6)] is only 3.87 kcal mol$^{-1}$ less stable than the Λ(λ)-*RR*(6) one, while the remaining geometries investigated possess much higher energies (9.0−33.7 kcal mol$^{-1}$). The NMR spectra of the Zn(II) complex indicate the presence of two species with $C_2$ symmetry in aqueous solution. Our calculations indicate that these two species correspond most likely to the Λ(λ)-*RR*(6) and Λ(δ)-*RR*(6) diasteroisomers, in which the metal ion is six-coordinated.

**Table 4.** C-PCM Relative Free Energies (kcal mol$^{-1}$) of the Different Diasteroisomeric Forms of [M(py-bcpe)] Complexes in Aqueous Solution

| | Zn | Cd | Pb | Ca |
|---|---|---|---|---|
| Λ(λ)-*RR*(6) | 0.00 | 0.00 | 3.24 | 7.48 |
| Λ(δ)-*RR*(6) | 3.87 | 3.68 | 1.17 | 9.76 |
| Λ(λ)*SS*(6) | 33.71 | 27.58 | 8.66 | 24.33 |
| Λ(δ)-*SS*(6) | 26.01 | 21.24 | 8.56 | 26.46 |
| Λ(λ)-*RS*(6) | 18.58 | 17.52 | 4.66 | 24.93 |
| Λ(δ)-*RS*(6) | 17.57 | 13.62 | 5.41 | 21.35 |
| Λ(λ)-*RR*(7) | 9.11 | 0.40 | 2.77 | 1.84 |
| Λ(δ)-*RR*(7) | 9.04 | 1.37 | 1.35 | 6.78 |
| Λ(λ)-*SS*(7) | 19.00 | 13.17 | 0.82 | 13.99 |
| Λ(δ)-*SS*(7) | 14.34 | 10.39 | 4.71 | 14.81 |
| Λ(λ)-*RS*(7) | 14.14 | 12.21 | 5.49 | 9.03 |
| Λ(δ)-*RS*(7) | 23.51 | 11.60 | 2.20 | 10.92 |
| Λ(λ)-*RR*(8) | 17.33 | 2.89 | 0.66 | 1.34 |
| Λ(δ)-*RR*(8) | 11.98 | 0.92 | 2.85 | 1.01 |
| Λ(λ)-*SS*(8) | 21.71 | 4.72 | 0.00 | 0.00 |
| Λ(δ)-*SS*(8) | 24.50 | 9.12 | 5.67 | 5.47 |
| Λ(λ)-*SR*(8) | *a* | 7.00 | 3.12 | 6.59 |
| Λ(δ)-*SR*(8) | 12.78 | 5.89 | 0.82 | 2.99 |

[a] The geometry optimization process led to the Λ(λ)-*SR*(7) form.

The ionic radius of Cd(II) [0.95 Å for CN 6] is substantially larger than that of Zn(II) [0.74 Å for CN 6],[47] and thus for [Cd(py-bcpe)] an important stabilization of geometries with CN 7 and 8 is expected in comparison to the situation observed for the Zn(II) analogue. Our calculations predict the Λ(λ)-*RR*(6) form to be the most stable one for the Cd(II) complex, as also predicted for the Zn(II) analogue (see Table 4). However, the Λ(λ)-*RR*(7) and Λ(δ)-*RR*(8) geometries are less stable than the former by only 0.40 and 0.92 kcal mol$^{-1}$, respectively. Thus, the complicated NMR spectra observed for the Cd(II) complex are probably due to the presence of different complex forms in solution with different coordination numbers.

The most stable geometry predicted by our calculations for the Ca(II) and Pb(II) complexes corresponds to the Λ(λ)-*SS*(8) form. This result is consistent with the NMR spectral data described above, which indicated a $C_2$ symmetry of these complexes in solution. The geometry observed for the Pb(II) complex in the solid state [Λ(δ)-*SR*(8)] is less stable than the Λ(λ)-*SS*(8) form by ∼0.8 kcal mol$^{-1}$. Moreover, inspection of the experimental and calculated geometries for the Λ(δ)-*SR*(8) geometry

(47) Shannon, R. D. *Acta Crystallogr.* **1976**, *A32*, 751–767.

indicates that the complex should provide a $C_1$ symmetry. Thus, our calculations most likely correctly predict the minimum energy geometry of the Pb(II) complex in solution, crystal packing forces being probably responsible for the stabilization of the $\Lambda(\delta)$-*SR*(8) structure observed in the solid state. This is also supported by the fact that the Ca(II) and Pb(II) complexes show very similar NMR spectra (see above).

**Stereochemical Activity of the Pb(II) Lone Pair.** The lack of predictability associated with the coordination chemistry of Pb(II) has been attributed to the interplay of electrostatic factors and ligand constraints that might permit the stereochemical activity of the Pb(II) lone pair. Shimoni-Livni et al.[40] investigated a close relation between the role of a lone pair of Pb(II) and the coordination geometry for a large number of Pb(II) complexes. They have found two general structural categories of Pb(II) compounds: holodirected and hemidirected, which are distinguished by the disposition of ligands around the metal ion. In the hemidirected form there is a void in the liganding that is not found in holodirected geometry. Complexes with high coordination numbers (9−10) usually adopt holodirected geometries, while lead(II) complexes with coordination numbers lower than 6 are normally hemidirected and have a stereochemically active lone pair. Both types of structures are found for intermediate coordination numbers (6−8). In this case, the stereochemical activity of the lone pair, and hence the geometry, seems to strongly depend on the nature of the donor atoms and the steric repulsion of the ligands. It has been stated that for electronegative donor atoms such as oxygen or nitrogen hemidirected structures are energetically favored.[40]

As discussed in the preceding section, our DFT calculations on the [Pb(py-bcpe)] system provide a minimum energy conformation that corresponds to the $\Lambda(\lambda)$-*SS*(8) form, with the conformation observed in the solid state [$\Lambda(\delta)$-*SR*(8)] being less stable than the latter by ∼0.8 kcal mol$^{-1}$. Table 5 lists the bond distances of the metal coordination environment calculated for the [Pb(py-bcpe)] complex by using DFT calculations. The calculated bond lengths for the $\Lambda(\delta)$-*SR*(8) form show a rather poor agreement with those observed experimentally, as evidenced by the agreement factor obtained ($AF_i$ = $[\sum(\text{exptl} - \text{calcd})^2/\sum(\text{exptl})^2]^{1/2}$ = 0.139, where exptl and calcd denote experimental and calculated values, respectively). For instance, a much better agreement factor is obtained in the case of the Zn(II) analogue [$AF_i$ = 0.057]. In particular, our calculations on the [Pb(py-bcpe)] system clearly overestimate the distances to the donor atoms of the ligand that are placed in the opposite site of the charged picolinate moieties [N(4) and N(5)], while the distances to the oxygen donor atoms of the picolinate moieties are clearly underestimated [O(1) and O(3)]. This suggests that in the calculated geometry, the stereochemical activity of the Pb(II) lone pair is much more important than in the solid state structure. Indeed, an analysis of the natural bond orbitals (NBOs) shows that the Pb(II) lone pair possesses a predominant 6s character, but it is polarized by a substantial 6p contribution: s[97.13%]p[2.87%]. Similar p contributions (1.89−4.39%) have been calculated for different hemidirected four-coordinate Pb(II) complexes with neutral ligands, while p contributions in the range 2.62−15.72% have been calculated for hemidirected four-coordinate Pb(II) complexes with anionic ligands.[40]

**Table 5.** Calculated (B3LYP/6-31G*) Bond Lengths (Å) of the Pb(II) Coordination Environment Obtained for the [Pb(py-bcpe)] System[a]

| | $\Lambda(\delta)$-*SR*(8) | | $\Lambda(\lambda)$-*SS*(8) | |
|---|---|---|---|---|
| | vacuo | solution | vacuo | solution |
| Pb−N(1) | 2.461 | 2.505 | 2.815 | 2.768 |
| Pb−N(2) | 2.966 | 2.802 | 3.217 | 2.995 |
| Pb−N(3) | 2.837 | 2.712 | 2.823 | 2.761 |
| Pb−N(4) | 3.411 | 3.135 | 3.217 | 2.995 |
| Pb−N(5) | 3.414 | 3.184 | 2.823 | 2.766 |
| Pb−N(6) | 2.918 | 2.824 | 2.815 | 2.766 |
| Pb−O(1) | 2.289 | 2.437 | 2.314 | 2.471 |
| Pb−O(3) | 2.288 | 2.443 | 2.314 | 2.471 |

[a] See Figure 5 for numbering scheme.

In a previous paper, we have demonstrated that hemidirected geometries might be favored by the presence in a polidentate ligand of donor atoms with a high charge density, which induce an important polarization of the Pb 6s lone pair.[41] The charge density distribution of dipolar compounds in the gas and in the condensed phase may be substantially different.[48] Thus, we have performed geometry optimizations of the [Pb(py-bcpe)] complex in aqueous solution (Figure 6). The bond distances of the metal coordination environment optimized in water are compared to those obtained in the gas phase in Table 5. In the case of the $\Lambda(\delta)$-*SR*(8) conformation, the inclusion of solvent effects results in a dramatic shortening of the Pb(1)−N(4) and Pb−N(5) bond distances (> 0.23 Å), while the distances to the donor atoms of the picolinate units O(1) and O(3) increase by ∼0.16 Å. These results suggest that the structure optimized in solution presents a lower degree of stereochemical activity of the Pb(II) lone pair, which is confirmed by the analysis of the NBOs: s[98.44%]p[1.56%]. This is attributed to a lower ability of the oxygen donor atoms of the picolinate units [O(1) and O(3)] to polarize the 6s Pb(II) lone pair in solution. The values of the natural charges obtained from natural population analysis (NPA) for O(1) and O(3) in the gas phase (−0.85) and in solution (−0.81) confirm this view.

The considerations concerning the effect of the solvent in the stereochemical activity of the $\Lambda(\delta)$-*SR*(8) form of the [Pb(py-bcpe)] complex also apply for the $\Lambda(\lambda)$-*SS*(8) conformation. Indeed, the inclusion of solvent effects during the geometry optimization process causes substantial changes in the bond distances of the metal coordination environment (Table 5). In particular, the bond distances to donor atoms placed on the opposite side with respect to the charged oxygen atoms of the picolinate units are shorter in water than in the gas-phase, while the Pb−O distances are clearly longer in solution (Figure 6). The inclusion of solvent effects also results in a lower degree of stereochemical activity of the Pb(II) lone pair: s[99.29%]p[0.71%] in the gas phase and s[99.92%]p[0.08%] in water. These results indicate that the complex is virtually holodirected in aqueous solution. Interestingly, our calculations performed in water indicate that the $\Lambda(\lambda)$-*SS*(8) conformation is more stable than the $\Lambda(\delta)$-*SR*(8) one by 1.84 kcal mol$^{-1}$,

(48) Monajjemi, M.; Chahkandi, B. *THEOCHEM* **2005**, *714*, 43–60.

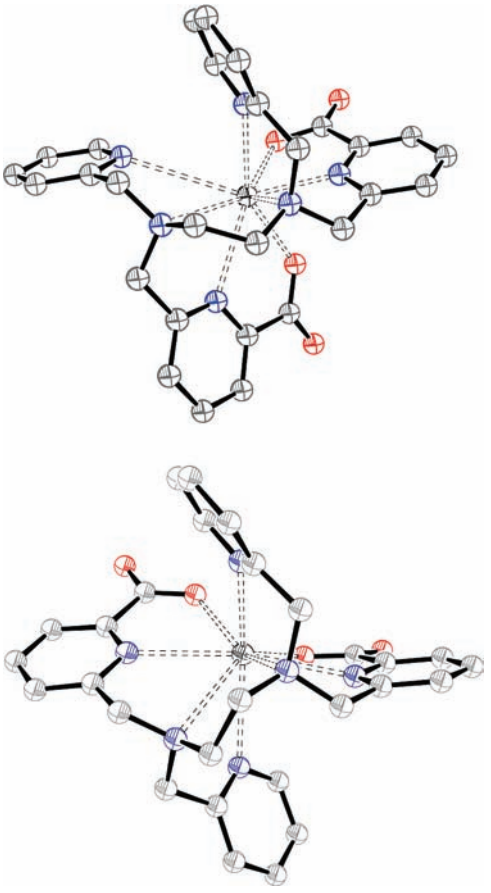

**Figure 6.** Molecular geometries of the Λ(δ)-*SR*(8) (top) and Λ(λ)-*SS*(8) (bottom) geometries of [Pb(py-bcpe)] obtained from DFT calculations in aqueous solution.

**Table 6.** Crystal Data and Structure Refinement for **1** and **2**

| | **1** | **2** |
|---|---|---|
| formula | $C_{28}H_{33.65}N_6O_{7.83}Zn$ | $C_{40}H_{60}Cl_2N_8O_{13}Pb$ |
| MW | 644.83 | 1139.05 |
| space group | $P\bar{1}$ | $P\bar{1}$ |
| crystal system | triclinicic | triclinicic |
| $a$/Å | 10.7910(6) | 13.666(1) |
| $b$/Å | 11.8384(7) | 13.780(1) |
| $c$/Å | 12.6031(7) | 15.627(1) |
| α/deg | 103.007(1) | 89.374(4) |
| $\beta$/deg | 94.263(1) | 66.353(3) |
| $\gamma$/deg | 109.660(1) | 61.903(3) |
| $V$/Å$^3$ | 1457.38(14) | 2319.7(3) |
| $Z$ | 2 | 2 |
| $T$/K | 100.0(2) | 100.0(2) |
| $\lambda$, Å (Mo Kα) | 0.71073 | 0.71073 |
| $D_{calcd}$/g cm$^{-3}$ | 1.469 | 1.631 |
| $\mu$/mm$^{-1}$ | 0.902 | 3.822 |
| $R_{int}$ | 0.0254 | 0.0346 |
| reflns measured | 7198 | 11491 |
| reflns observed | 6313 | 10626 |
| $R_1$[a] | 0.0304 | 0.0218 |
| $wR_2$ (all data)[b] | 0.0795 | 0.0611 |

[a] $R_1 = \sum||F_0| - |F_c||/\sum|F_0|$. [b] $wR_2 = \{\sum[w(|F_0|^2 - |F_c|^2)^2]/\sum[w(F_0^4)]\}^{1/2}$

in line with the relative energies obtained from solvated single point energy calculations on the geometries optimized in the gas-phase (Table 4). Thus, we conclude that the [Pb(py-bcpe)] complex adopts a holodirected Λ(λ)-*SS*(8) conformation in aqueous solution.

## Conclusions

The octaadentate ligand py-bcpe forms Ca(II), Zn(II), Cd(II), and Pb(II) complexes in aqueous solution, and the stability of these complexes is higher than that of the corresponding edta analogues. Our results show that the introduction of the pyridyl pendants in bcpe provides a certain selectivity for Cd(II) and Pb(II) over Zn(II), while keeping good Pb(II)/Ca(II) and Cd(II)/Ca(II) selectivities. Thus, py-bcpe can be considered as a new structural framework for the design of novel Cd(II) and Pb(II) extracting agents. A detailed investigation of the structure in aqueous solution of the [M(py-bcpe)] complexes shows that the Zn(II) complex is six-coordinated, while the Ca(II) and Pb(II) analogues are eight-coordinated. In the case of the Cd(II) complex, the NMR data, together with theoretical calculations performed at the DFT level, suggest that both six- and seven-coordinated species exist in aqueous solution. The [Pb(py-bcpe)] complex adopts a holodirected Λ(λ)-*SS*(8) conformation in aqueous solution, in spite of the hemidirected Λ(δ)-*SR*(8) conformation observed in the solid state. The results shown in this Article also highlight the importance of including solvent effects to obtain a more accurate description of the solution geometries of Pb(II) complexes. The inclusion of solvent effects appears to be particularly important for complexes with ligands containing charged donor atoms, as their charge density distribution, and therefore their ability to polarize the Pb(II) 6s lone pair, may be substantially different in the gas phase and in solution.

## Experimental Section

**Chemicals and Starting Materials.** 1,2-Bis{[[6-(methoxycarbonyl)pyridin-2-yl]methyl]amino}-ethane (**1**, Scheme 1) was prepared as previously reported by us.[25] All other chemicals were purchased from commercial sources and used without further purification. Solvents were of reagent grade purified by the usual methods.

***Caution!*** *Although we have experienced no difficulties with the perchlorate salts, these should be regarded as potentially explosive and handled with care.*[49]

**6,6′-(Ethane-1,2-diylbis((pyridine-2-ylmethyl)azanediyl))bis-(methylene)dipicolinic Acid.** 1,2-Bis{[[6-(methoxycarbonyl)-pyridin-2-yl]methyl]amino}-ethane (1.070 g, 2.99 mmol) was dissolved in acetonitrile (100 mL), and $Na_2CO_3$ (10.0 g, 94.35 mmol) and 2-bromomethylpyridine dibromohydrate (1.60 g, 6.33 mmol) were added. The mixture was refluxed for 48 h, and then the excess $Na_2CO_3$ was filtered off. The filtrate was evaporated to dryness to give a reddish oil that was purified on a silica column eluting with $CH_3CN/H_2O$/saturated aqueous $KNO_3$ (14:2:1). The fractions containing the product were concentrated to dryness, and the residue was partitioned between $H_2O$ and $CHCl_3$. The organic phase was dried over $Na_2SO_4$ and concentrated to dryness. The residue was dissolved in 6 M aqueous HCl (20 mL) and refluxed for 48 h. The yellow precipitate formed was isolated by filtration and dried under vacuum to give 0.632 g of the desired product (yield, 30%). Anal. Calcd for $C_{28}H_{28}N_6O_4 \cdot 4HCl \cdot 3H_2O$: C, 47.20; H, 5.38; N, 11.80. Found: C, 46.97; H, 5.37; N, 11.72. Fast atom bombardment-mass spectrometry (FAB-MS) ($m/z$(% base peak intensity (BPI))): 513(75) [py-$H_3$bpce]$^+$. IR (KBr): 1716 $\nu$(C=O), 1611 $\nu$(C=N), 1594 $\nu$(C=C) cm$^{-1}$. A portion of the py-$H_2$bpce·4HCl·3$H_2O$ ligand (0.183 g, 0.257 mmol) was converted to the hydronitrate form by reaction with $AgNO_3$ (0.180 g, 1.060 mmol) in water (10 cm$^3$). The AgCl precipitate

(49) Wolsey, W. C. *J. Chem. Educ.* **1973**, *50*, A335–A337.

was filtered off and the filtrate concentrated to dryness to provide 0.069 g of py-$H_2$bpce·$4HNO_3$·$4H_2O$ as a yellow solid. Anal. Calcd for $C_{28}H_{28}N_6O_4$·$4HNO_3$·$4H_2O$: C, 40.19; H, 4.82; N, 16.74. Found: C, 39.75; H, 4.33; N, 16.37.

**Physical Methods.** Elemental analyses were carried out on a Carlo Erba 1180 elemental analyzer and FAB-MS were recorded on a Thermo MAT95XP mass spectrometer using 3-nitrobenzyl alcohol as the matrix. IR spectra were recorded, as KBr discs, using a Bruker Vector 22 spectrophotometer. $^1$H and $^{13}$C NMR spectra were run on Bruker Avance 300 or Bruker Avance 500 spectrometers. Chemical shifts are reported in $\delta$ values. For measurements in $D_2O$, *tert*-butyl alcohol was used as an internal standard with the methyl signal calibrated at $\delta = 1.2$ ($^1$H) and 31.2 ppm ($^{13}$C). Spectral assignments were based in part on two-dimensional COSY, HMQC, and HMBC experiments. Samples of the Zn(II), Cd(II), Pb(II), and Ca(II) complexes for NMR measurements were prepared by dissolving equimolar amounts of the ligand and hydrated $M(ClO_4)_2$ (M = Zn, Cd, or Ca) or $Pb(NO_3)_2$ in $D_2O$, followed by adjustment of the pD with $ND_4OD$ and DCl (Aldrich) solutions in $D_2O$.

**Potentiometric Measurements.** Ligand protonation constants and stability constants with Zn(II), Cd(II), Pb(II), and Ca(II) were determined by pH-potentiometric titration at 25 °C in 0.1 M tetramethylammonium nitrate. The titrations were carried out adding a standardized tetramethylammonium hydroxide solution with a Metrohm Dosimat 794 automatic buret. A glass electrode filled with 3 M KCl was used to measure pH. The stock solutions were prepared by dilution of the appropriate standards. The exact amount of acid present in the standard solutions was determined by pH measurement. Tetramethylammonium hydroxide was standardized by potentiometric titration against potassium hydrogen phthalate. The ligand was checked for purity by NMR and elemental analysis before titration. The ligand and metal−ligand (1:1) solutions were titrated over the pH range $2.0 < pH < 11.0$. The protonation and stability constants were calculated from simultaneous fits of three independent titrations with the program HYPERQUAD.[50] The errors given correspond to 1 standard deviation.

**Computational Methods.** The [M(py-bcpe)] systems (M = Zn, Cd, Pb, or Ca) were fully optimized by using the B3LYP density functional model.[51,52] In these calculations we have used the standard 6-31G(d) basis set for the ligand atoms, while the LanL2DZ valence and effective core potential functions were used for the metals.[46] The stationary points found on the potential energy surfaces as a result of the geometry optimizations of the complexes have been tested to represent energy minima rather than saddle points via frequency analysis. In aqueous solution relative free energies of the different conformations of [M(py-bcpe)] complexes were calculated from solvated single-point energy calculations on the geometries optimized in vacuo. With the use of frequency calculations, the zero-point energies and the thermal corrections together with the entropies were calculated in order to convert the internal energies to the Gibbs energies at 298.15 K. The solvation energies were computed in order to convert the gas-phase energies to the energies in the solution phase.[53] Hydration free energies were evaluated by using the polarizable continuum model (PCM). In particular, we used the C-PCM variant[54] that employs conductor rather than dielectric boundary conditions. The solute cavity is built as an envelope of spheres centered on atoms or atomic groups with appropriate radii. Calculations were performed using an average area of 0.2 Å$^2$ for all the finite elements (tesserae) used to build the solute cavities. Final free energies of reaction include both electrostatic and nonelectrostatic contributions. Selected conformations of the [Pb(py-bcpe)] complex were fully optimized in aqueous solution by using the C-PCM. The wave functions of the Pb complexes were analyzed by natural bond orbital analyses, involving natural atomic orbital (NAO) populations and natural bond orbitals (NBO).[55,56] All DFT calculations were performed by using the Gaussian 03 program package (revision C.01).[57]

**X-ray Crystal Structure Determinations.** Crystals of formula [Zn(py-bcpe)]·$3.83H_2O$ (**1**) were obtained by slow evaporation at room temperature of a solution of the complex prepared by dissolving py-$H_2$bpce·$4HCl·3H_2O$ (0.0100 g, 0.013 mmol) and $Zn(ClO_4)_2·6H_2O$ (0.0045 g, 0.012 mmol) in $D_2O$ (1 mL) followed by adjustment of the pD to 6.2 with $ND_4OD$. Crystals of formula [Pb(py-bcpe)]·$2Et_3NHClO_4·H_2O$ (**2**) were obtained by dissolving py-$H_2$bpce·$4HCl·3H_2O$ (0.056 g, 0.071 mmol), triethylamine (0.080 mL, 0.574 mmol), and $Pb(ClO_4)_2·3H_2O$ (0.031 g, 0.076 mmol) in methanol (10 mL). The solution was concentrated to 2 mL and diethylether (5 mL) was added. Upon standing for a few days single crystals of **2** suitable for X-ray diffraction were obtained. Three dimensional X-ray data were collected on a Bruker X8 APEXII CCD. Data were corrected for Lorentz and polarization effects and for absorption by semi-empirical methods[58] based on symmetry-equivalent reflections. Complex scattering factors were taken from the program SHELX97[59] running under the WinGX program system[60] as implemented on a Pentium computer. Both structures were solved by direct methods (SIR92[61]) and refined[59] by full-matrix least-squares on $F^2$. All hydrogen atoms were included in calculated positions and refined in riding mode in both compounds, except those of the water molecules that were located in a difference electron-density map and all the parameters fixed. Both crystals present positional disorder that were solved; compound **2** presents disorder on a perchlorate anion with occupancy factors of 0.62(1) for O10A, O11A, and O12A. Compound **1** presents disorder on a pyridine pendant and one of the water molecules with occupancy factors for major positions of 0.826(3). Refinement converged with anisotropic displacement parameters for all non-hydrogen atoms. Crystal data

(50) Gans, P.; Sabatini, A.; Vacca, A. *Talanta* **1996**, *43*, 1739–1753.
(51) Becke, A. D. *J. Chem. Phys.* **1993**, *98*, 5648–5652.
(52) Lee, C.; Yang, W.; Parr, R. G. *Phys. Rev. B* **1988**, *37*, 785–789.
(53) Nuñez, C.; Mato-Iglesias, M.; Bastida, R.; Macias, A.; Perez-Lourido, P.; Platas-Iglesias, C.; Valencia, L. *Eur. J. Inorg. Chem.* **2009**, 1086–1095.
(54) Barone, V.; Cossi, M. *J. Phys. Chem. A* **1998**, *102*, 1995–2001.
(55) Glendening, E. D.; Reed, A. E.; Carpenter, J. E.; Weinhold, F. *NBO*, version 3.1; 1998.
(56) Reed, A. E.; Curtiss, L. A.; Weinhold, F. *Chem. Rev.* **1988**, *88*, 899–926.
(57) Frisch, M. J.; Trucks, G. W.; Schlegel, H. B.; Scuseria, G. E.; Robb, M. A.; Cheeseman, J. R.; Montgomery, J. A., Jr.; Vreven, T.; Kudin, K. N.; Burant, J. C.; Millam, J. M.; Iyengar, S. S.; Tomasi, J.; Barone, V.; Mennucci, B.; Cossi, M.; Scalmani, G.; Rega, N.; Petersson, G. A.; Nakatsuji, H.; Hada, M.; Ehara, M.; Toyota, K.; Fukuda, R.; Hasegawa, J.; Ishida, M.; Nakajima, T.; Honda, Y.; Kitao, O.; Nakai, H.; Klene, M.; Li, X.; Knox, J. E.; Hratchian, H. P.; Cross, J. B.; Bakken, V.; Adamo, C.; Jaramillo, J.; Gomperts, R.; Stratmann, R. E.; Yazyev, O.; Austin, A. J.; Cammi, R.; Pomelli, C.; Ochterski, J. W.; Ayala, P. Y.; Morokuma, K.; Voth, G. A.; Salvador, P.; Dannenberg, J. J.; Zakrzewski, V. G.; Dapprich, S.; Daniels, A. D.; Strain, M. C.; Farkas, O.; Malick, D. K.; Rabuck, A. D.; Raghavachari, K.; Foresman, J. B.; Ortiz, J. V.; Cui, Q.; Baboul, A. G.; Clifford, S.; Cioslowski, J.; Stefanov, B. B.; Liu, G.; Liashenko, A.; Piskorz, P.; Komaromi, I.; Martin, R. L.; Fox, D. J.; Keith, T.; Al-Laham, M. A.; Peng, C. Y.; Nanayakkara, A.; Challacombe, M.; Gill, P. M. W.; Johnson, B.; Chen, W.; Wong, M. W.; Gonzalez, C.; Pople, J. A. *Gaussian 03*, revision C.01; Gaussian, Inc.: Wallingford, CT, **2004**.
(58) *SABADS, Bruker-AXS*, version 2004/1; Bruker AXS Inc.: Madison, WI, 2004.
(59) SHELX: Sheldrick, G. M. *Acta Crystallogr.* **2008**, *A64*, 112–122.
(60) WinGX MS-Windows system of programs for solving, refining and analysing single crystal X-ray diffraction data for small molecules: Farrugia, L. J. *J. Appl. Crystallogr.* **1999**, *32*, 837−838.
(61) SIR92: Altomare, A.; Cascarano, G.; Giacovazzo, C.; Guagliardi, A.; Burla, M. C.; Polidori, G.; Camalli, M. *J. Appl. Crystallogr.* **1994**, *27*, 435.

and details on data collection and refinement are summarized in Table 6.

**Acknowledgment.** The authors thank Xunta de Galicia (Grants PGIDIT06TAM10301PR and INCITE08ENA103005ES) for generous financial support. The authors are indebted to Centro de Supercomputación of Galicia (CESGA) for providing the computer facilities.

**Supporting Information Available:** Figure S1 showing potentiometric titration curves, Figure S2 showing absorption spectra of py-bcpe recorded at different pH values, in vacuo optimized Cartesian coordinates (Å) for the [M(py-bcpe)] complexes (M = Zn, Cd, Pb or Ca), and X-ray crystallographic data in CIF format for compounds **1** and **2**. This material is available free of charge via the Internet at http://pubs.acs.org.